Lanthanoid/Alkali Metal β-Triketonate Assemblies: A Robust Platform for Efficient NIR Emitters

Mr. Brodie L. Reid,[a] Dr. Stefano Stagni,[b] Dr. Joanna M. Malicka,[c] Dr. Massimo Cocchi,[c,d] Dr. Alexandre N. Sobolev,[e] Prof. Brian W. Skelton,[e] Dr. Evan G. Moore,[f] Prof. Garry S. Hanan,[g] Prof. Mark I. Ogden,*[a] and Dr. Massimiliano Massi*[a]

[a] *Department of Chemistry, and Nanochemistry Research Institute, Curtin University, Kent Street, Bentley 6102 WA, Australia.*

[b] *Department of Industrial Chemistry "Toso Montanari" – University of Bologna, viale del Risorgimento 4, Bologna 40126, Italy.*

[c] *Laboratory of Micro and Submicro Enabling Technologies of Emilia-Romagna Region S.c.r.l. (MIST E-R S.c.r.l.), via Gobetti 101, 40129 Bologna, Italy.*

[d] *Institute for Organic Synthesis and Photoreactivity, CNR, via Gobetti 101, 40129 Bologna.*

[e] *Centre for Microscopy, Characterisation and Analysis, University of Western Australia, Crawley 6009 WA, Australia.*

[f] *School of Chemistry and Molecular Biosciences, University of Queensland, St Lucia 4072 QLD, Australia.*

[g] *Department of Chemistry, D-600 Université de Montréal, 2900 Edouard-Montpetit Montréal, Quebec, Canada.*

Corresponding Authors

*E-mail: m.massi@curtin.edu.au; m.ogden@curtin.edu.au.

Keywords: lanthanides, luminescence, triketonates, diketonates, near-infrared.

Abstract

The reaction of hydrated lanthanoid chlorides with tribenzoylmethane and an alkali metal hydroxide consistently resulted in the crystallization of neutral tetranuclear assemblies of formulation $[Ln(Ae{\cdot}HOEt)(\mathbf{L})_4]_2$ (Ln = Eu^{3+}, Er^{3+}, Yb^{3+}; Ae = Na^+, K^+, Rb^+). Analysis of the crystal structures of these species revealed a coordination geometry that varied from slightly distorted square antiprismatic to slightly distorted triangular dodecahedron, with the specific geometrical shape being dependent on the degree of lattice solvation and identity of the alkali metal. The near-infrared (NIR) emitting assemblies of Yb^{3+} and Er^{3+} showed remarkably efficient emission, characterized by significantly longer excited-state lifetimes (τ_{obs} ~ 40-47 μs for Yb^{3+} and τ_{obs} ~ 4-6 μs for Er^{3+}) when compared to the broader family of lanthanoid β-diketonate species, even in the case of perfluorination of the ligands. The Eu^{3+} assemblies possess bright red emission and a luminescence performance (τ_{obs} ~ 0.5 ms, Φ^{L}_{Ln} ~ 35-37%, η_{sens} ~ 68-70%) more akin to the β-diketonate species. The results highlight that the β-triketonate ligand offers a tuneable and facile system for the preparation of efficient NIR-emitters, without the need for more complicated perfluorination or deuteration synthetic strategies.

Introduction

The luminescent properties of the lanthanoid trivalent cations are useful in a wide range of applications.[1–7] In particular, complexes of these elements that exhibit emission in the near-infrared (NIR) region have been highly sought after in the biomedical area,[2,8–10] as NIR photons offer deeper tissue penetration and are less affected by scattering.[11] NIR emission is also used in optical devices such as night-vision technologies and in telecommunication.[9,12–15] The great challenge in the design of efficient NIR emitting lanthanoid complexes is quenching of the excited-state *via* multiphonon relaxation caused by high frequency stretching vibrations such as OH, NH, and CH bonds.[16–18] Given that, in general, organic sensitizing chromophores are required to bypass the poor molar absorptivity of direct lanthanoid excitation, it is rather complicated to deplete the lanthanoid complexes of these types of bonds, which are common in organic molecules. Attempts to remove such quenching pathways include the synthesis of ligands with less of such high frequency oscillators,[19–21] as well as dissolution of lanthanoid complexes in deuterated solvents.[22,23] Strategies such as perfluorination and quantitative deuteration of ligands have been explored with success to

minimize the extent of quenching and improve the NIR emission of lanthanoid complexes,[24,25] especially in the case of ligands belonging to the β-diketonate class.[26–29] Lanthanoid β-diketonate complexes have been proven to be robust, thermally stable, and suitable for applications in materials science.[30–32] However, synthetic routes towards perfluorinated ligands are significantly more complicated and somewhat hinder ligand design, and deuteration facilities are not routinely accessible within synthetic chemistry laboratories.

We have reported the photophysical properties of a novel tetranuclear assembly, $[Yb(K{\cdot}HOEt)(\mathbf{L})_4]_2$, where the $\mathbf{L}^-$ ligand is the β-triketonate tribenzoylmethanide.[33] Given the considerably detailed investigation of lanthanoid β-diketonate complexes to date,[34] it was surprising that the β-triketonate analogues were rather unexplored. Only a couple of reports in the late sixties described the emissive properties of lanthanoid β-triketonate complexes without any structural studies.[35–37] Remarkably, the $[Yb(K{\cdot}HOEt)(\mathbf{L})_4]_2$ assembly proved to be a highly efficient NIR emitter when compared to the photophysical performance of NIR-emitting lanthanoid β-diketonate complexes. Furthermore, we were able to demonstrate that the photophysical properties of such an assembly can be exploited in the emitting layer of Organic Light Emitting Diodes fabricated by sublimation. Our preliminary investigation demonstrated that the performance of these NIR-OLEDs outclassed any previously reported NIR-OLED based on lanthanoid complexes.

We have now extended our investigation to determine if these tetranuclear assemblies can be formed with other lanthanoid (Ln) and alkali element (Ae) metal cations. In particular, we have focussed on the NIR emitting Yb^{3+} and Er^{3+} cations, in combination with Na^+, K^+ and Rb^+ cations. The results demonstrate that this tetranuclear assembly is extremely robust. Furthermore, the photophysical data show that these assemblies are consistent highly efficient NIR emitters, with photophysical properties second only to complexes where perfluorination *and* deuteration strategies had been used in the preparation of β-diketonate ligands. As a comparison, we have also synthesized the Eu^{3+}/Ae^+ analogues, which were found to be bright red-emitters, albeit characterized by a photophysical performance typical of β-diketonate complexes.

Results and Discussion

Synthesis of the tetranuclear assemblies

The robustness of the assembly structure to variations in the alkali metal and lanthanoid cation was investigated. The tribenzoylmethane ligand **L**H (2-benzoyl-1,3-diphenyl-1,3-propandione) was prepared as previously reported, by treatment of dibenzoylmethane with NaH and benzoyl chloride in diethyl ether.[33] The synthesis of the tetranuclear assemblies $[Ln(Ae{\cdot}HOEt)(\mathbf{L})_4]_2$ was trialled following the previously reported method for isolation of $[Yb(K{\cdot}HOEt)(\mathbf{L})_4]_2$, where **L**H is reacted with a hydrated lanthanoid chloride in ethanol and in the presence of alkali metal hydroxides (Figure 1).[33] For each Ln^{3+}/Ae^{+} combination (Ln^{3+} = Eu^{3+}, Er^{3+}, Yb^{3+}; Ae^{+} = Na^{+}, K^{+}, Rb^{+}), structural investigation by X-ray diffraction revealed the targeted $[Ln(Ae{\cdot}HOEt)(\mathbf{L})_4]_2$ assembly. Changing the solvent from ethanol to *n*-butanol was also trialled using Eu^{3+} and K^{+}, which yielded the analogous $[Eu(K{\cdot}HOBu)(\mathbf{L})_4]_2$ assembly. Based on these results, this family of tetranuclear assemblies is remarkably robust, with the observed structure being maintained while systematically changing the lanthanoid, the alkali metal, or the alcoholic solvent. Aside from X-ray diffraction studies, the complexes were analyzed by means of IR spectroscopy and elemental analyses. The latter, in particular, revealed the presence of variable degrees of lattice solvent molecules, consistent with the structure determinations.

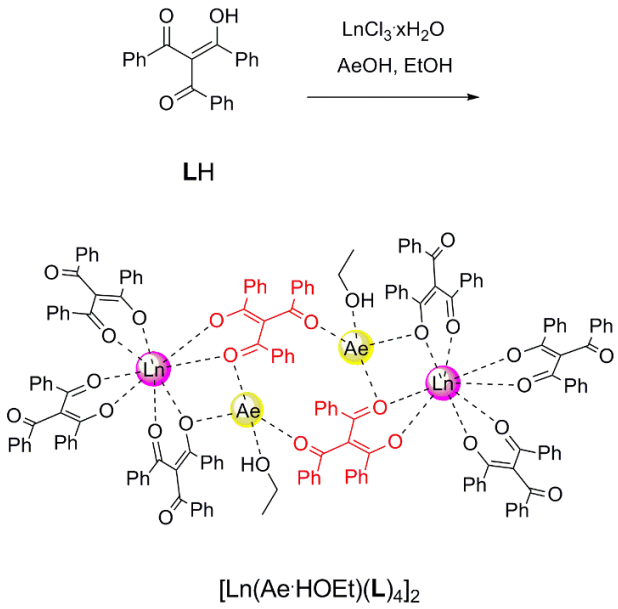

Figure 1 – Synthetic pathway to lanthanoid assemblies bearing β-triketonate ligands. Ln^{3+} = Eu^{3+}, Er^{3+}, Yb^{3+}; Ae^{+} = Na^{+}, K^{+}, Rb^{+}.

X-ray diffraction studies and coordination geometries

The formally neutral $[Ln(Ae{\cdot}HOEt)(\mathbf{L})_4]_2$ assemblies illustrated herein are analogous to the previously reported $[Yb(K{\cdot}HOEt)(\mathbf{L})_4]_2$ (Figure 2 and Figures S1-S9). However, it was determined that, along with unsolvated structures, the assemblies can also crystallize as different solvates including; $[Ln(Ae{\cdot}HOEt)(\mathbf{L})_4]_2{\cdot}2(EtOH)$, and $[Ln(Ae{\cdot}HOEt)(\mathbf{L})_4]_2{\cdot}2(H_2O)(EtOH)$. In fact, for $[Yb(K{\cdot}HOEt)(\mathbf{L})_4]_2$, both the unsolvated and solvated structures have now been identified by single crystal X-ray diffraction, the latter incorporating two molecules of water and one of ethanol (for a comparison of solvate structures see Supporting Information, Figure S10). The $[Eu(K{\cdot}HOBu)(\mathbf{L})_4]_2$ assembly crystallized as a solvate of formula $[Eu(K{\cdot}HOBu)(\mathbf{L})_4]_2{\cdot}2(H_2O)(BuOH)$, but the core structure of the assembly does not seem to be strongly influenced by the change in the coordinated alcohol molecules.

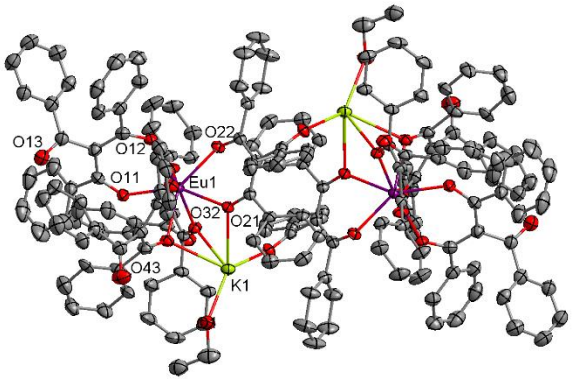

Figure 2 – Plot of $[Eu(K{\cdot}HOEt)(\mathbf{L})_4]_2$, with displacement ellipsoids drawn at the 50% probability level. Hydrogen atoms and solvent molecules have been omitted for clarity.

Interestingly, it was noted that the presence (or absence) and the nature of the lattice solvent molecules as well as the identity of the Ae^+ cation have a non-negligible influence on the specific geometry of the coordination environment around the lanthanoid center. In fact, four different geometrical arrangements have been identified through an analysis of all the crystal structures reported herein. The specific geometries vary from slightly distorted square antiprismatic to slightly distorted triangular dodecahedron (Figure 3). The variation of the

geometries between square antiprismatic and triangular dodecahedron was assessed and confirmed using Shape Version 2.1 software (see Supporting Information, Table S1).[38,39]

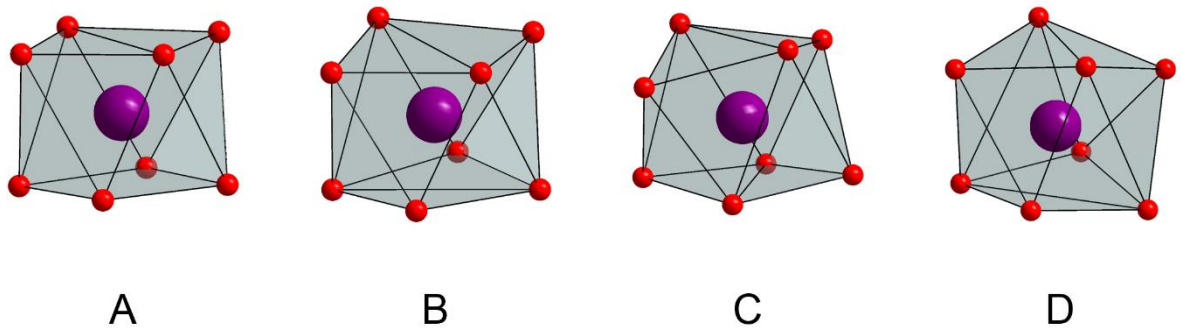

Figure 3 - View of the various geometries from distorted square antiprismatic (A) towards distorted triangular dodecahedron (D). The coordination A corresponds to the unsolvated $[Ln(Na{\cdot}HOEt)(\mathbf{L})_4]_2$ assemblies (Ln^{3+} = Eu^{3+}, Yb^{3+}, and Er^{3+}. B corresponds to the unsolvated $[Ln(Ae{\cdot}HOEt)(\mathbf{L})_4]_2$ (Ln^{3+}/Ae^{+} = Er^{3+}/Rb^{+}, Yb^{3+}/K^{+},[33] and Yb^{3+}/Rb^{+}). C corresponds to solvated $[Ln(Ae{\cdot}HOEt)(\mathbf{L})_4]_2{\cdot}2(H_2O)(EtOH)$ (Ln^{3+}/Ae^{+} = Er^{3+}/K^{+}, Yb^{3+}/K^{+}). D corresponds to solvated $[Ln(Ae{\cdot}HOEt)(\mathbf{L})_4]_2{\cdot}2(EtOH)$ (Ln^{3+}/Ae^{+} = Eu^{3+}/K^{+}, Eu^{3+}/Rb^{+}).

From an analysis of the structures, it becomes evident that all the unsolvated species bearing Na^{+} have a coordination geometry that is the closest to square antiprismatic, irrespective of the lanthanoid cation. From this arrangement, a slight distortion is observed for the unsolvated structures bearing Er^{3+}/Rb^{+}, Yb^{3+}/K^{+},[33] and Yb^{3+}/Rb^{+}. Further distortion is evident for the Er^{3+}/K^{+} and Yb^{3+}/K^{+} structures that appear solvated by two molecules of water and one of ethanol. Lastly, closer to a triangular dodecahedron, lie the Eu^{3+}/K^{+} and Eu^{3+}/Rb^{+} assemblies with two lattice ethanol molecules.

As it might be expected, the $[Eu(K{\cdot}HOBu)(\mathbf{L})_4]_2$ assembly is different from any of the other assemblies, highlighting a Eu^{3+} coordination that is somewhat more distorted from both regular polyhedra (see Supporting Information, Table S1).[38]

Selected bond distance values are reported in Table 1. The average Ln-O distance decreases from Eu^{3+} (~2.38 Å) to Yb^{3+} (~2.30 Å), consistent with considerations based on the lanthanoid contraction. The Ln···Ln distance is always greater than 8.70 Å, which is long

enough to suggest that direct energy migration between the two lanthanoid centers within the assembly should not be occurring.[40]

Table 1 – Selected distances (Å) between the two lanthanoid cations (Ln···Ln) within the tetranuclear assemblies, between the lanthanoid centers and the ethanol/*n*-butanol OH group (Ln···OH), and average Ln-O bond distances within the first coordination sphere. Grouped by the geometry of the coordination in Figure 3.

Geometry	Assembly	Ln···Ln	Ln···OH	Ave. Ln-O
A	$[Eu(Na{\cdot}HOEt)(\mathbf{L})_4]_2$	8.980	4.355	2.383
	$[Er(Na{\cdot}HOEt)(\mathbf{L})_4]_2$	8.925	4.339	2.324
	$[Yb(Na{\cdot}HOEt)(\mathbf{L})_4]_2$	8.917	4.359	2.305
B	$[Er(Rb{\cdot}HOEt)(\mathbf{L})_4]_2$	8.813	6.062	2.325
	$[Yb(K{\cdot}HOEt)(\mathbf{L})_4]_2$ [*a*]	8.804	5.720	2.304
	$[Yb(Rb{\cdot}HOEt)(\mathbf{L})_4]_2$	8.792	6.080	2.303
C	$[Er(K{\cdot}HOEt)(\mathbf{L})_4]_2$	9.145	6.239	2.316
	$[Yb(K{\cdot}HOEt)(\mathbf{L})_4]_2$	9.128	6.252	2.299
D	$[Eu(K{\cdot}HOEt)(\mathbf{L})_4]_2$	8.968	5.861	2.380
	$[Eu(Rb{\cdot}HOEt)(\mathbf{L})_4]_2$	8.949	6.096	2.381
Other	$[Eu(K{\cdot}HOBu)(\mathbf{L})_4]_2$	9.271	6.297	2.382

[*a*] crystal structure reported previously.[33]

The position of the ethanol (or *n*-butanol) molecule coordinated to the Ae^+ cation is of relevance, as the high frequency of the OH oscillator may provide outer sphere multiphonon relaxation pathways that are able to quench the lanthanoid excited-states. The shortest Ln···OH distances are present in the assemblies bearing Na^+ (~4.5-5.0 Å), as the Na^+ cation binds to two μ-O atoms bridging to the Ln^{3+}, while the larger K^+ and Rb^+ ions bind to three μ-O bridged atoms. The Na^+ ion is small enough to allow the ethanol OH to engage in a hydrogen bonding interaction with the third μ-O atom, while the K^+ and Rb^+ complexes effectively disallow this interaction (see Supporting Information, Figure S10). The Ln···OH distances slightly increase in the assemblies bearing the larger Rb^+ ion compared to the K^+ ion (K^+, 5.60-5.70 Å; Rb^+, 6.00-6.10 Å).

Photophysical Investigation

The triplet $^3\pi\pi^*$ excited-state of $\mathbf{L}^-$ was previously reported to be at 20,704 cm^{-1},[33] which is of a sufficient energy to sensitize the metal-centered emission of Yb^{3+}, Er^{3+} and Eu^{3+}. All of the assemblies reported in this work were found to be emissive either in the NIR or visible region (Figure 4; for photos of all emissions - see Supporting Information, Figures S11-S12). In each case, the emission originates as a consequence of the antenna effect, as indicated by the broad excitation profiles between 250 and 500 nm (see Supporting Information, Figures S14-S15, S18-S20, S24-S27) analogous to the absorption spectrum of the $\mathbf{L}^-$ ligand in ethanol (see Supporting Information, Figure S13). All the emission spectra were found to be independent from the excitation wavelength.

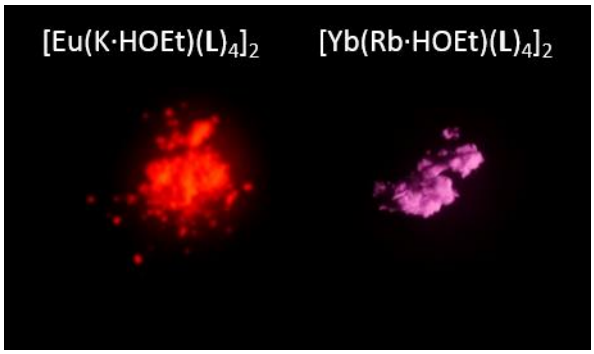

Figure 4 – Solid state emission of $[Eu(K{\cdot}HOEt)(\mathbf{L})_4]_2$ (left) and $[Yb(Rb{\cdot}HOEt)(\mathbf{L})_4]_2$ (right) after excitation at 350 nm. Cut-on filter is 550 nm for Eu^{3+}, and 900 nm for Yb^{3+}. The NIR emission of Yb^{3+} was captured by removing the infrared filter from the camera to allow wavelengths above 700 nm to be detected by the photodiode.

Photophysical Properties of the NIR emitting Yb^{3+} and Er^{3+} assemblies in the solid state

The energy difference between the ligand $^3\pi\pi^*$ state and the $^2F_{5/2}$ Yb^{3+} excited-state is ~10,454 cm^{-1}, which should favor an efficient energy transfer.[41,42] In the case of Yb^{3+}, energy *transfer via* a ligand-to-metal charge transfer state might also be occurring.[43,44] Characteristic NIR fluorescent emission was observed from the $[Yb(Ae{\cdot}HOEt)(\mathbf{L})_4]_2$ (Ae^+ = Na^+ and Rb^+) assemblies in the 900-1100 nm region (Figure 5), analogously to the reported $[Yb(K{\cdot}HOEt)(\mathbf{L})_4]_2$.[33] The emission is attributed to the $^2F_{7/2}\leftarrow{}^2F_{5/2}$ transition, which is split into four main observable bands due to crystal field effects.[16] The high energy shoulder around 950 nm in the emission spectra can be attributed to emission from "hot" excited-

states.[45] Slight differences in the relative intensities in the bands are ascribed to the various degree of distortion in the coordination geometries.

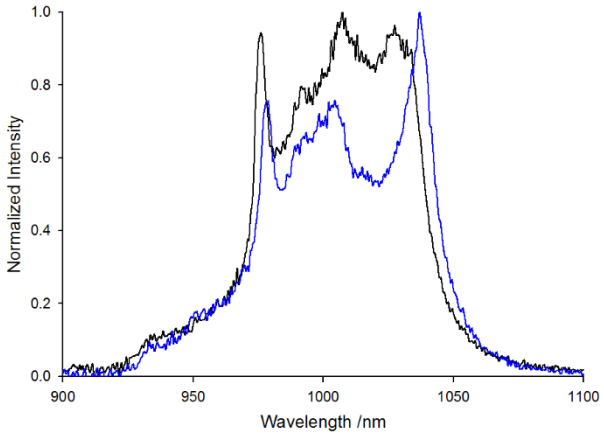

Figure 5 - Solid state normalized emission spectra (λ_{ex} = 350 nm) of the [Yb(Ae·HOEt)(**L**)$_4$]$_2$ assemblies. Ae^+ = Na^+ (blue trace) and Rb^+ (black trace). The emission profile of [Yb(K·HOEt)(**L**)$_4$]$_2$ was reported elsewhere.[33]

Table 2 – Selected photophysical data of NIR emitting Ln^{3+}/Ae^+ complexes in the solid state.

	τ_{obs} (µs)	Φ^{Ln}_{Ln} (%)[a]
[Yb(Na·HOEt)(**L**)$_4$]$_2$	37.0	3.1
[Yb(K·HOEt)(**L**)$_4$]$_2$[b]	46.7	3.9
[Yb(Rb·HOEt)(**L**)$_4$]$_2$	44.4	3.8
[Er(Na·HOEt)(**L**)$_4$]$_2$	4.8	0.7
[Er(K·HOEt)(**L**)$_4$]$_2$	5.0	0.8
[Er(Rb·HOEt)(**L**)$_4$]$_2$	5.8	0.9

[*a*] Intrinsic quantum yields were calculated using τ_R values of 1.2 ms for Yb^{3+} and 0.66 ms[16] for Er^{3+}. [*b*] Previously reported values.[33]

The excited-state lifetime (τ_{obs}) for [Yb(Ae·HOEt)(**L**)$_4$]$_2$ (Ae^+ = Na^+ and Rb^+) were fit to a monoexponential function, giving values of 37.0 µs and 44.4 µs, respectively (see Supporting

Information, Figures S16-S17). These values (reported in Table 2) are significantly long-lived and amongst the longest recorded for solid state Yb^{3+} species bound to β-diketonate ligands, for which typical values are ~5 μs.[29] The values of τ_{obs} for the assemblies reported herein are even longer than those of complexes whose ligands were perfluorinated to reduce the extent of multiphonon relaxation caused by CH bonds (~12 μs).[27] Only complexes bearing perfluorinated *and* deuterated β-diketonate ligands appear to have values of τ_{obs} longer than the family of $[Yb(Ae{\cdot}HOEt)(\mathbf{L})_4]_2$ assemblies (from 47 μs at 53% deuteration, to 289 μs at 96% deuteration at the α-C position),[28] albeit at the expense of more complicated and often not readily available synthetic capabilities. Assuming a radiative lifetime (τ_R) value of 1.2 ms, which is standard for Yb^{3+} β-diketonate complexes,[46,47] the intrinsic quantum yields (Φ^{Ln}_{Ln}) can be approximated to 3.1 and 3.8% for the Na^+ and Rb^+-bearing assemblies, respectively. Following the trend reported for τ_{obs}, these values are amongst the highest recorded Φ^{Ln}_{Ln} for the Yb^{3+} β-diketonate family in the solid state, indicating the efficiency of the $[Yb(Ae{\cdot}HOEt)(\mathbf{L})_4]_2$ assemblies in preventing quenching *via* multiphonon relaxation.

The $[Er(Ae{\cdot}HOEt)(\mathbf{L})_4]_2$ ($Ae^+ = Na^+$, K^+ and Rb^+) assemblies also display fluorescent NIR emission in the 1420-1620 nm range, which is attributed to the characteristic $^4I_{15/2} \leftarrow {}^4I_{13/2}$ transition (Figure 6). The band appears narrow and structured as a result of crystal field effects.[26] Again, the structure of the emission band varies slightly due to the relatively different crystal field effects present in the three assemblies. The excitation spectra, along with the typical broad antenna component, also show a sharp transition at 485 nm consistent with the spin-allowed $^4I_{15/2} \rightarrow {}^4F_{7/2}$ intraconfigurational transition.[48]

The values of τ_{obs} were fit to a monoexponential decay of 4.8, 5.0, and 5.8 μs for $[Er(Ae{\cdot}HOEt)(\mathbf{L})_4]_2$ with $Ae^+ = Na^+$, K^+ and Rb^+, respectively (Table 2, see Supporting Information, Figures S21-S23). As per the case of the Yb^{3+} assemblies, these τ_{obs} values are longer than those found with perfluorinated Er^{3+} β-diketonate complexes (~1-2 μs)[26] and are, to the best of our knowledge, only outclassed in cases when the β-diketonate ligand has been both perfluorinated *and* deuterated (from ~6 μs at 58% deuteration, to ~11 μs at 98% deuteration at the α-C position).[28] Therefore, the advantageous reduction of multiphonon relaxation observed in the case of Yb^{3+} is consistently maintained for the Er^{3+} assemblies.

The values of τ_{obs} for the Na^+-bearing assemblies of Yb^{3+} and Er^{3+} are shortened by ~20% when compared to their analogous assemblies incorporating either K^+ or Rb^+. This effect is tentatively attributed to more efficient quenching caused by the closer proximity of the

ethanolic OH groups in the Na^{+}-containing structures, as illustrated by the X-ray diffraction studies.

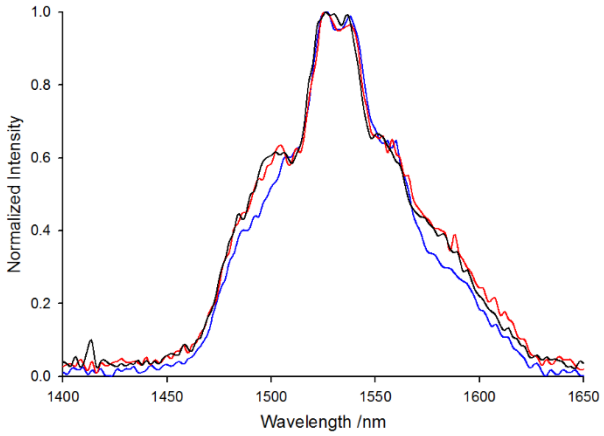

Figure 6 - Normalized emission spectra of $[Er(Na{\cdot}HOEt)(\mathbf{L})_4]_2$ (blue trace, λ_{ex} = 380 nm), $[Er(K{\cdot}HOEt)(\mathbf{L})_4]_2$ (red trace, λ_{ex} = 370 nm), and $[Er(Rb{\cdot}HOEt)(\mathbf{L})_4]_2$ (black trace, λ_{ex} = 400 nm) in the solid state.

Overall, the photophysical data demonstrate that the $[Ln(K{\cdot}HOEt)(\mathbf{L})_4]_2$ assemblies represent a family of efficient and bright NIR-emitting species in the case of Yb^{3+} and Er^{3+}. Clearly, the major observed factor for the improvement of the luminescence performance seems to be associated with the removal of quenching effects from the α-CH in the β-triketonate $\mathbf{L}^{-}$ ligand. This new class of β-triketonate ligand may offer a viable and more facile synthetic approach to ligand design for lanthanoid NIR-emitting complexes, without the need to rely exclusively on perfluorination and deuteration strategies.

Photophysical properties of the red emitting Eu^{3+} assemblies in the solid state

All of the Eu^{3+} assemblies display the characteristic Eu^{3+}-centered line-like emission between 580 and 750 nm (Figure 7). The triplet state energy of the $\mathbf{L}^{-}$ antenna lies 1,704 cm^{-1} above the Eu^{3+} $^5D_1$ excited-state, which is known to be an efficient energy difference to allow energy transfer to both the $^5D_1$ and $^5D_0$ states.[49] In each excitation spectrum, there is a sharp band at 465 nm, consistent with an intraconfigurational $^7F_0 \rightarrow {}^5D_2$ transition.[16]

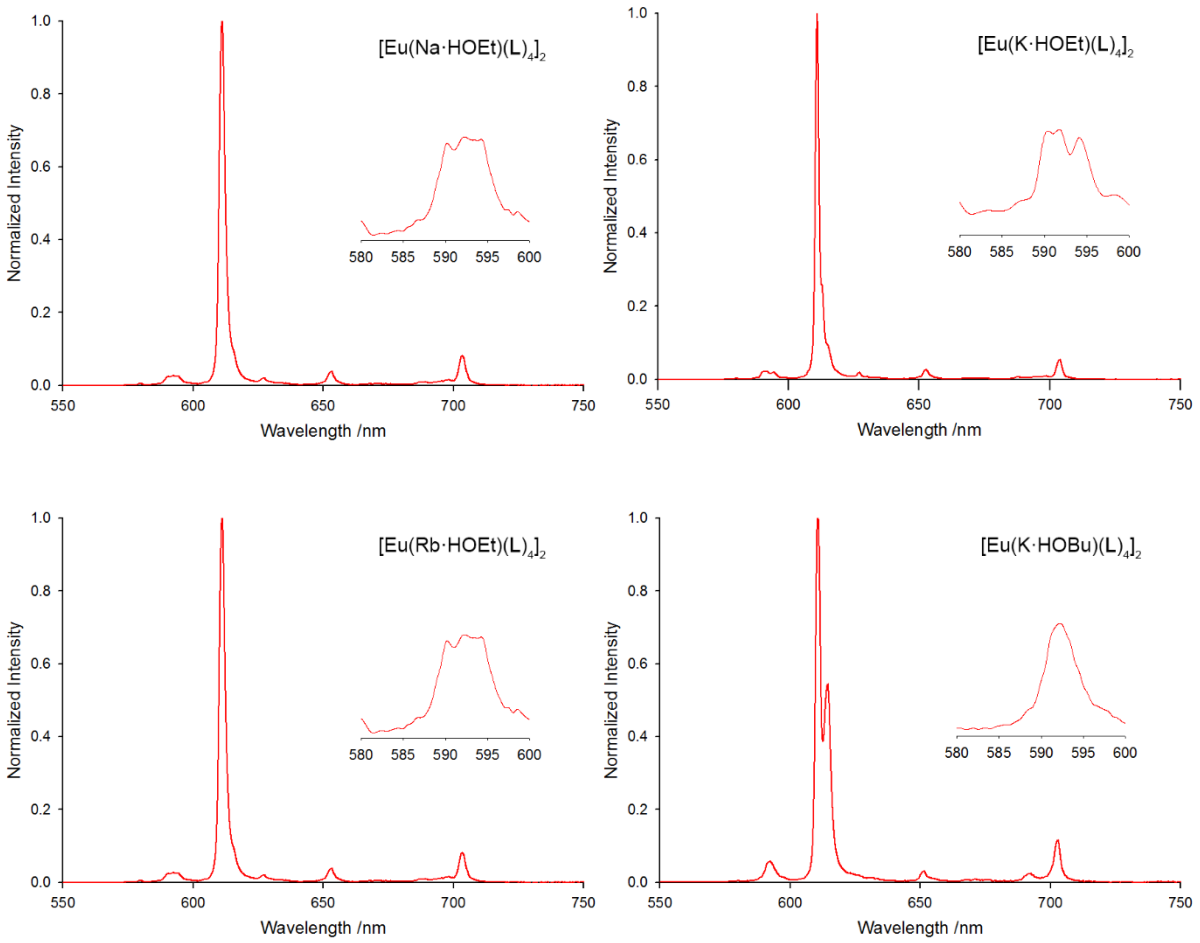

Figure 7 - Normalized emission spectra of $[Eu(Na{\cdot}HOEt)(\mathbf{L})_4]_2$, $[Eu(K{\cdot}HOEt)(\mathbf{L})_4]_2$, $[Eu(Rb{\cdot}HOEt)(\mathbf{L})_4]_2$, and $[Eu(K{\cdot}HOBu)(\mathbf{L})_4]_2$ in the solid state (λ_{ex} = 350 nm). Inset: Close-up of the splitting in the $^7F_1 \longleftarrow {}^5D_0$ emission band.

The spectra display five distinct bands corresponding to the $^7F_J \longleftarrow {}^5D_0$ (J = 0-4) transitions. The profiles of the emission spectra are very similar between all the Eu^{3+} assemblies, however slight differences in the fine structure of the bands are consistent with the presence of the various degrees of distortion identified in the crystal structures.

The weak $^7F_0 \longleftarrow {}^5D_0$ band has a full-width-half-maximum (FWHM) ranging between 15 and 59 cm^{-1}, apart from the $[Eu(K{\cdot}HOBu)(\mathbf{L})_4]_2$ complex, for which a value could not be estimated due to the low intensity. This range is consistent with one unique emitting Eu^{3+} for each assembly,[50] in agreement with the fact that the two Eu^{3+} are related by an inversion centre located in the centre of the assembly and therefore have identical coordination geometries.

The magnetically allowed $^7F_1 \leftarrow ^5D_0$ transition is virtually superimposable for the Eu^{3+}/K^+ and Eu^{3+}/Rb^+ assemblies, consistent with identical coordination geometries. The splitting pattern of three peaks, with the two lower energy ones being quasi-degenerate is consistent with the slightly distorted D_{2d} symmetry of the coordination observed in the crystal structure. On the other hand, the splitting pattern of the $^7F_1 \leftarrow ^5D_0$ transition in the Na^+-bearing assembly is different, as it presents three peaks with the two higher energy ones being quasi-degenerate. This pattern is in agreement with a slightly distorted square antiprismatic D_{4d} symmetry.[51,52] The $[Eu(K{\cdot}HOBu)(\mathbf{L})_4]_2$ assembly displays a single broad peak devoid of structure, which might be an indication that the bulk sample is obtained as a mixture of differently solvated structures.

The integration of the hypersensitive $^7F_2 \leftarrow ^5D_0$ transition was compared to that of the $^7F_1 \leftarrow ^5D_0$ transition, whose intensity is unaffected by the crystal field, to give an $I(^7F_2 \leftarrow ^5D_0)/I(^7F_1 \leftarrow ^5D_0)$ = 15.49, 15.68, 16.03, and 12.76, for $[Eu(Na{\cdot}HOEt)(\mathbf{L})_4]_2$, $[Eu(K{\cdot}HOEt)(\mathbf{L})_4]_2$, $[Eu(Rb{\cdot}HOEt)(\mathbf{L})_4]_2$, and $[Eu(K{\cdot}HOBu)(\mathbf{L})_4]_2$, respectively. The ratio is quite large in each case, which might be due to the distorted coordination geometries promoting partial relaxation of the parity-forbidden nature of the transition *via J*-mixing and/or crystal field mixing.[53]

Lifetime decay and quantum yield data for the Eu^{3+} assemblies are reported in Table 3. The values of τ_{obs} were found to be consistently in the 500-540 μs range (Figures S28-S31), with overall quantum yields (Φ^L_{Ln}) measured to be in the 35-37% range. The radiative lifetimes could be calculated directly from the emission spectra, obtaining values in the 1.01-1.22 ms range. From these data, the intrinsic quantum yields (Φ^{Ln}_{Ln}) were determined to be around 50%, leading to sensitization efficiencies (η_{sens}) of the $\mathbf{L}^-$ ligands in 68-73% range. Therefore, $\mathbf{L}^-$ is an efficient sensitizer for Eu^{3+} luminescence. Despite the fact that the ethanolic OH group lies closer to the Eu^{3+} centers in the Na^+ assembly, there does not appear to be a greater degree of multiphonon relaxation as observed for the case of Yb^{3+} and Er^{3+}. The lack of quenching in this case may be due to the fact that OH is a less efficient quencher of the Eu^{3+} excited-state in comparison to Er^{3+} and Yb^{3+}, or that the OH is engaged in hydrogen bonding, making it a non-efficient quencher for Eu^{3+}-centered emission.[16] Overall the photophysical data indicate that the β-triketonate assemblies of Eu^{3+} are efficient and bright red emitters, although their performance is akin to that observed for the β-diketonate complexes in the solid state, with no major improvement as observed for the Yb^{3+} and Er^{3+} NIR-emitters.[34]

Table 3 - Selected photophysical data of Eu^{3+} complexes in the solid state and in an ethanolic solution at 298K and 77K.

	τ_{obs} (ms)	τ_R (ms)[a]	Φ^{Ln}_{Ln} (%)	Φ^{L}_{Ln} (%)	η_{sens} (%)
$[Eu(Na\cdot HOEt)(L)_4]_2$					
Solid	0.50	1.01	50	35	70
298K [77K]	0.15 [0.41]	1.16 [1.16]	13 [36]		
$[Eu(K\cdot HOEt)(L)_4]_2$					
Solid	0.52	1.03	50	37	73
298K [77K]	0.18 [0.43]	1.15 [1.11]	16 [39]		
$[Eu(Rb\cdot HOEt)(L)_4]_2$					
Solid	0.54 (77%), 0.37 (23%)	1.02[b]	53[b]	36	68
298K [77K]	0.18 [0.43]	1.16 [1.15]	16 [37]		
$[Eu(K\cdot HOBu)(L)_4]_2$					
Solid	0.51 (87%) 0.18 (13%)	1.22[b]	42[b]		

[a] Radiative lifetime calculated assuming a refractive index of 1.50 for the solid state.[54,55] [b] Calculated using the major τ_{obs} component.

The assemblies were found to be scarcely soluble in alcoholic solvents such as ethanol and methanol, albeit soluble enough to conduct photophysical measurements. On the other hand, they were found to be insoluble in either water or other common organic solvents. The emission spectra and photophysical data of the Eu^{3+} (Table 3) and Yb^{3+} assemblies in ethanol solution were found to be significantly altered (see Supporting Information, Figures S32-S44). As in the case of the previously investigated $[Yb(K\cdot HOEt)(\mathbf{L})_4]_2$,[33] these differences

may be ascribed to the lability of the lanthanoid and alkali metal cations, thus promoting ligand exchange in ethanol solution.

To further probe the stability of the assemblies in alcoholic solvents, the number of alcohol molecules coordinated to the Eu^{3+} center in solution was determined by a comparison of the Eu^{3+} excited-state lifetime in methanol and deuterated methanol, using the method proposed by Horrocks[56]. The $[Eu(K{\cdot}HOEt)(\mathbf{L})_4]_2$ assembly was used as a representative exemplar. The measured excited-state lifetime values were $\tau(CH_3OH)$ = 125 μs and $\tau(CD_3OD)$ = 153 μs. These values indicate that about three molecules of methanol are directly coordinated to the Eu^{3+} center in solution, providing further evidence that the structure of the assembly is not preserved (for photophysical data, see Supporting Information, Figures S45-S47). Although we have previously demonstrated that this new class of β-triketonate assemblies can be used as precursors for the sublimation of optically active materials in the fabrication of NIR-OLEDs,[33] solution processing techniques are hindered by the low solubility of the assemblies. An effort is now underway to make this class of compounds more soluble in non-polar solvent by ligand design, an approach that has previously been successful in the chemistry of lanthanoid-hydroxo clusters.[57]

Conclusion

Tetranuclear $[Ln(Ae{\cdot}HOEt)(\mathbf{L})_4]_2$ complexes of tribenzoylmethane have been synthesized and shown to persist for a range of different metal combinations. The coordination geometry around the lanthanoid cation is subtly altered, in the solid state at least, by the nature of the alkali metal cation and the degree of solvation present in the crystal lattice. The photophysical properties of the NIR emitting complexes of Yb^{3+} and Er^{3+} are particularly promising, significantly exceeding the performance of comparable β-diketonate complexes in the solid state, except where such ligands are both perfluorinated *and* deuterated. The Eu^{3+} tetranuclear analogues are bright red-emitters, but with performance similar to β-diketonate complexes. Solution-phase studies in alcohols showed that the tetranuclear complexes do not persist in polar solvents. Work is now underway to modify the β-triketonate ligands to improve the solubility of the tetranuclear complexes in non-polar solvents.

Experimental Section

General procedures

All reagents and solvents were purchased from chemical suppliers and used as received without further purification. The ligand, 2-benzoyl-1,3-diphenyl-1,3-propandione (**L**H), was prepared as we have previously reported.[33] Hydrated $LnCl_3$ was prepared by the reaction of Ln_2O_3 with hydrochloric acid, followed by evaporation of the solvent under reduced pressure. The $[Yb(K{\cdot}HOEt)(\mathbf{L})_4]_2$ complex was prepared according to our previously published procedure.[33] Infrared spectra (IR) were recorded on solid state samples using an attenuated total reflectance Perkin Elmer Spectrum 100 FT-IR. IR spectra were recorded from 4000 to 650 cm^{-1}; the intensities of the IR bands are reported as strong (s), medium (m), or weak (w), with broad (br) bands also specified. Melting points were determined using a BI Barnsted Electrothermal 9100 apparatus. Elemental analyses were obtained at either Curtin University (Australia), or the elemental analysis services at the University of Tasmania (Australia).

Photos of the Eu^{3+} red emissions were captured using a Nikon D300 equipped with an aperture of f/9, and an OG550 EOS barrier filter. NIR emissions of Yb^{3+} complexes were captured using a Canon 40D with its infrared filter removed to allow wavelengths above 700 nm to be detected by the photodiode. The camera was equipped with a RM90 barrier filter, with an exposure time of five seconds.

Selected Equations

Using the observed lifetimes (τ_{obs}) and calculated quantum yields (Φ^{L}_{Ln}); values of the radiative lifetime (τ_R), and intrinsic quantum yield (Φ^{Ln}_{Ln}), can be calculated following methods proposed by Werts *et al*.[46]

$$\frac{1}{\tau_R} = 14.65\ s^{-1} \times\ n^3\ \times \frac{I_{Tot}}{I_{MD}} \qquad \text{(equation 1)}$$

In equation 1, the refractive index (n) of the solvent is used (assumed value of 1.5 in the solid state),[54,55] The value 14.65 s^{-1} is the spontaneous emission probability of the $^7F_1 \leftarrow {}^5D_0$ transition reported previously.[58] I_{Tot} is the total integration of the Eu^{3+} emission spectrum, and I_{MD} is the integration of the $^7F_1 \leftarrow {}^5D_0$ transition.

$$\Phi^{Ln}_{Ln} = \frac{\tau_{obs}}{\tau_R} \qquad \text{(equation 2)}$$

The sensitization efficiency (η_{sens}) can be determined using equation 3 below:

$$\eta_{sens} = \frac{\Phi_{Ln}^{L}}{\Phi_{Ln}^{Ln}} \qquad \text{(equation 3)}$$

Photophysical Measurements

Absorption spectra were recorded at room temperature using a Perkin Elmer Lambda 35 UV/Vis spectrometer. Uncorrected steady state emission and excitation spectra were recorded using an Edinburgh FLSP980-stm spectrometer equipped with a 450 W xenon arc lamp, double excitation and emission monochromators, a Peltier cooled Hamamatsu R928P photomultiplier (185–850 nm) and a Hamamatsu R5509-42 photomultiplier for detection of NIR radiation (800-1400 nm). Emission and excitation spectra were corrected for source intensity (lamp and grating) and emission spectral response (detector and grating) by a calibration curve supplied with the instrument. Quantum yields were measured with the use of an integrating sphere coated with BenFlect.

Excited-state decays (τ) were recorded on the same Edinburgh FLSP980-stm spectrometer using a microsecond flashlamp the above-mentioned R928P PMT photomultiplier as the detector. The goodness of fit was assessed by minimizing the reduced χ^2 function and by visual inspection of the weighted residuals.

To record the luminescence spectra at 77 K, the samples were placed in quartz tubes (2 mm diameter) and inserted in a special quartz Dewar filled with liquid nitrogen. All the solvents used in the preparation of the solutions for the photophysical investigations were of spectrometric grade.

General Synthesis of $[Ln(Ae{\cdot}HOEt)(L)_4]_2$

To a mixture of **L**H (68-72 mg, 0.21 mmol) and hydrated $LnCl_3$ (20 mg), an aqueous AeOH solution (1 M, 206-218 μL, 0.21 mmol) was added. Ethanol (10 ml) was added and the mixture heated at reflux for 30 minutes. The resulting mixture was filtered and the filtrate left to stand at ambient temperature. Slow evaporation of the solvent over several days afforded yellow crystals (10-40 mg).

[*Eu(Na·HOEt)(L)$_4$]$_2$*

M.p. 268-270°C; elemental analysis calcd (%) for $C_{180}H_{132}Eu_2Na_2O_{26}$·1.5($H_2O$): C 70.63; H 4.35; found: C 69.68; H 4.11; ATR-IR: ν = 3647 w, 3559 w, 3058 w, 3027 w, 2976 w, 1646 m, 1596 w, 1583 s, 1542 s, 1491 m, 1448 s, 1368 s, 1311 w, 1277 w, 1270 m, 1179 w, 1150 w, 1073 w, 1053 w, 1027 w, 999 w, 975 w, 898 m, 823 w, 779 s, 746 s, 694 s, 669 s cm^{-1}.

[Eu(K·HOEt)(L)$_4$]$_2$

M.p. 244-246°C; elemental analysis calcd (%) for $C_{180}H_{132}Eu_2K_2O_{26}$·($H_2O$): C 69.90; H 4.30; found: C 69.13; H 3.93; ATR-IR: ν = 3644 w, 3568 w, 3057 w, 3024 w, 1645 m, 1610 w, 1584 s, 1543 s, 1491 m, 1448 m, 1370 s, 1311 m, 1278 m, 1180 w, 1151 m, 1073 w, 1027 w, 1013 w, 999 w, 925 w, 898 m, 823 w, 780 w, 748 m, 694 m, 669 w cm^{-1}.

[*Eu(K·HOBu)(L)$_4$]$_2$*

M.p. 238-240°C; elemental analysis calcd (%) for $C_{184}H_{140}Eu_2K_2O_{26}$: C 70.18; H 4.48; found: C, 70.43; H, 4.79; ATR-IR: ν = 3405 br w, 3057 w, 3027 w, 2959 w, 2932 w, 2870 w, 1593 m, 1546 s, 1509 s, 1476 s, 1461 m, 1441 w, 1416 m, 1282 w, 1219 w, 1180 w, 1154 w, 1060 w, 1022 w, 987 w, 940 w, 811 w, 782 w, 752 w, 719 m, 690 w cm^{-1}.

[Eu(Rb·HOEt)(L)$_4$]$_2$

M.p. 247-248°C; elemental analysis calcd (%) for $C_{180}H_{132}Eu_2Rb_2O_{26}$: C 67.86; H 4.18; found: C 67.48; H 4.07; ATR-IR: ν = 3647 w, 3567 w, 3057 w, 3025 w, 1646 m, 1584 s, 1543 s, 1488 m, 1448 m, 1369 s, 1311 m, 1276 m, 1178 w, 1152 m, 1073 w, 1027 w, 1014 w, 999 w, 975 w, 927 w, 898 m, 823 w, 780 w, 749 m, 694 m, 669 w cm^{-1}.

[*Er(Na·HOEt)(L)$_4$]$_2$*

M.p. 276-278°C; elemental analysis calcd (%) for $C_{180}H_{132}Er_2Na_2O_{26}$·2($H_2O$): C 69.13; H 4.38; found: C, 69.68; H, 3.88; ATR-IR: ν = 3652 w, 3557 w, 3058 w, 2021 w, 2979 w, 1646 m, 1612 w, 1584 s, 1547 s, 1491 m, 1447 s, 1373 s, 1311 s, 1271 m, 1150 m, 1072 w, 1052w, 1027 w, 1013 w, 998 w, 978 w, 933 w, 923 w, 899 m, 823 w, 780 s, 747 s, 694 s, 669 s cm^{-1}.

[Er(K·HOEt)(L)$_4$]$_2$

M.p. 244-246°C; an accurate elemental analysis could not be achieved for this complex possibly due to the presence of multiple solvates; ATR-IR: ν = 3654 w, 3573 w, 3057 w, 3022 w, 1646 m, 1615 w, 1584 s, 1546 s, 1493 m, 1449 m, 1372 s, 1315 m, 1277 m, 1183 w, 1152 m, 1074 w, 1030 w, 1017 w, 998 w, 973 w, 930 w, 898 m, 827 w, 780 w, 749 m, 698 m, 670 w cm^{-1}.

[Er(Rb·HOEt)(L)$_4$]$_2$

M.p. 242-244°C; elemental analysis calcd (%) for $C_{180}H_{132}Er_2Rb_2O_{26}·0.5(H_2O)$: C 67.03; H 4.16; found: C 66.70; H 3.73; ATR-IR: ν = 3643 w, 3057 w, 1645 m, 1615 w, 1584 s, 1546 s, 1492 m, 1448 m, 1372 s, 1311 m, 1277 m, 1182 w, 1152 m, 1073 w, 1027 w, 1014 w, 1002 w, 980 w, 925 w, 897 m, 823 w, 780 w, 749 m, 694 m, 668 w cm^{-1}.

[*Yb(Na·HOEt)(L)$_4$]$_2$*

M.p. 260-262°C; elemental analysis calcd (%) for $C_{180}H_{132}Yb_2Na_2O_{26}·3(H_2O)$: C 68.48; H 4.41; found: C 68.37; H 4.09; ATR-IR: ν = 3643 w, 3555 w, 3054 w, 2921 w, 2853 w, 1645 m, 1613 w, 1590 s, 1547 s, 1490 m, 1441 s, 1397 w, 1364 s, 1328 w, 1294 w, 1270 m, 1181 w, 1154 w, 1093 w, 1073 w, 1029 w, 998 w, 932 w, 900 m, 824 w, 783 s, 754 s, 695 s, 671 s cm^{-1}.

[Yb(Rb·HOEt)(L)$_4$]$_2$

Crystals appear as pale yellow needles; m.p. 244-245°C; elemental analysis calcd (%) for $C_{180}H_{132}Yb_2Rb_2O_{26}$: C 66.98; H 4.12; found: C 66.80; H 3.97; ATR-IR: ν = 3635 w, 3468 w, 3057 w, 3020 w, 1643 m, 1611 w, 1585 s, 1548 s, 1492 m, 1448 m, 1374 s, 1311 m, 1277 m, 1177 w, 1153 m, 1073 w, 1027 w, 1014 w, 999 w, 975 w, 929 w, 898 m, 824 w, 780 w, 749 m, 694 m, 669 w cm^{-1}.

X-ray Crystallography

Crystallographic data for the structures were collected at 100(2) K on an Oxford Diffraction Gemini or Xcalibur diffractometer fitted with Mo Kα or Cu Kα radiation**.** Following absorption corrections and solution by direct methods, the structures were refined against F^2 with full-matrix least-squares using the program SHELXL-97 or SHELX-2014.[59]

Unless stated below, anisotropic displacement parameters were employed for the non-hydrogen atoms. All hydrogen atoms were added at calculated positions and refined by use of a riding model with isotropic displacement parameters based on those of the parent atom. CCDC-1401028 [Eu(Na·HOEt)(**L**)$_4$]$_2$, CCDC-1401029 [Eu(K·HOEt)(**L**)$_4$]$_2$, CCDC-1401030 [Eu(K·HOBu)(**L**)$_4$]$_2$, CCDC-1401031 [Eu(Rb·HOEt)(**L**)$_4$]$_2$, CCDC-1401033 [Er(Na·HOEt)(**L**)$_4$]$_2$, CCDC-1401034 [Er(K·HOEt)(**L**)$_4$]$_2$, CCDC-1401035 [Er(Rb·HOEt)(**L**)$_4$]$_2$, CCDC-1401036 [Yb(Na·HOEt)(**L**)$_4$]$_2$, CCDC-1401037 [Yb(K·HOEt)(**L**)$_4$]$_2$, and CCDC-1401038 [Yb(Rb·HOEt)(**L**)$_4$]$_2$ contain supplementary

crystallographic data, and can be obtained free of charge *via* http://www.ccdc.cam.ac.uk/conts/retrieving.html, or from the Cambridge Crystallographic Data Centre, 12 Union Road, Cambridge CB2 1EZ, U.K.; fax: (+44) 1223-336-033; or e-mail: deposit@ccdc.cam.ac.uk

X-ray data refinement

[Eu(Na·HOEt)(L)$_4$]$_2$. Empirical formula $C_{180}H_{132}Eu_2Na_2O_{26}$; *MW* = 3060.79. λ = 0.71073 Å. Triclinic, Space group $P\bar{1}$, *a* = 13.8309(3), *b* = 14.6650(3), *c* = 18.1873(4) Å, α = 104.903(2)°, β = 90.612(2)°, γ = 90.238(2)°, Volume = 3564.55(13) Å^3, *Z* = 1; ρ_c = 1.426 Mg/m^3, μ = 0.955 mm^{-1}, crystal size 0.21 x 0.14 x 0.05 mm^3; $\theta_{min,\ max}$ = 3.58, 32.71°. Reflections collected = 51951, unique reflections = 23685 [*R*(int) = 0.0519]. Max./min. transmission = 1.00/0.947. Number of parameters = 946, S = 1.005. Final *R* indices [$I>2\sigma(I)$] *R*1 = 0.0490, *wR*2 = 0.1003; *R* indices (all data) *R*1 = 0.0675, *wR*2 = 0.1084. Largest diff. peak and hole = 4.845 and -1.972 e. Å^{-3}.

[Eu(K·HOEt)(L)$_4$]$_2$·2EtOH. Empirical formula $C_{184}H_{144}Eu_2K_2O_{28}$; *MW* = 13185.10. λ = 1.54178 Å. Triclinic, Space group $P\bar{1}$, *a* = 13.9581(4), *b* = 14.8305(5), *c* = 19.6602(7) Å, α = 80.186(3)°, β = 72.466(3)°, γ = 90.124(3)°, Volume = 3817.7(2) Å^3, *Z* = 1; ρ_c = 1.385 Mg/m^3, μ = 6.914 mm^{-1}, crystal size 0.275 x 0.105 x 0.05 mm^3; $\theta_{min,\ max}$ = 2.40, 67.31°. Reflections collected = 36759, unique reflections = 13559 [*R*(int) = 0.0594]. Max./min. transmission = 0.718 and 0.247. Number of parameters = 1069, S = 1.038. Final *R* indices [$I>2\sigma(I)$] *R*1 = 0.0542, *wR*2 = 0.1403; *R* indices (all data) *R*1 = 0.0621, *wR*2 = 0.1482. Largest diff. peak and hole = 2.414 and -0.905 e. Å^{-3}. One phenyl ring, and both the coordinated and uncoordinated ethanol solvent molecules were modelled as being disordered over two sets of sites with occupancies constrained to 0.5 after trail refinement.

[Eu(K·HOBu)(L)$_4$]$_2$·2(H$_2$O)(BuOH). Empirical formula $C_{188}H_{154}Eu_2K_2O_{29}$; *MW* = 3259.22. λ = 0.71073 Å. Triclinic, Space group $P\bar{1}$, *a* = 14.5832(5), *b* = 16.4263(5), *c* = 18.3874(7) Å, α = 63.817(3)°, β = 89.549(3)°, γ = 82.095(3)°, Volume = 3908.2(3) Å^3, *Z* = 1; ρ_c = 1.385 Mg/m^3, μ = 0.924 mm^{-1}, crystal size 0.47 x 0.39 x 0.13 mm^3; $\theta_{min,\ max}$ = 2.08, 30.00°. Reflections collected = 59227, unique reflections = 22751 [*R*(int) = 0.0442]. Max./min. transmission = 0.900 and 0.735. Number of parameters = 1075, S = 1.040. Final *R* indices [$I>2\sigma(I)$] *R*1 = 0.0433, *wR*2 = 0.1016; *R* indices (all data) *R*1 = 0.0584, *wR*2 = 0.1093. Largest diff. peak and hole = 2.148 and -1.008 e. Å^{-3}. Two phenyl rings were modelled as being disordered over two sets of sites with occupancies refined to 0.732(6) and its

complement. The atoms of the minor components were refined with isotropic displacement parameters. The solvent was modelled as an *n*-butanol disordered about an inversion center and a water molecule on general positions.

[Eu(Rb·HOEt)(L)$_4$]$_2$·2EtOH. Empirical formula $C_{184}H_{144}Eu_2O_{28}Rb_2$; *MW* = 3277.84. λ = 0.71073 Å. Triclinic, Space group $P\bar{1}$, *a* = 14.0028(3), *b* = 14.7844(3), *c* = 19.7354(4) Å, α = 80.113(2)°, β = 72.448(2)°, γ = 90.143(2)°, Volume = 3831.20(14) Å^3, *Z* = 1; ρ_c = 1.421 Mg/m^3, μ = 1.517 mm^{-1}, crystal size 0.29 x 0.26 x 0.19 mm^3; $\theta_{min,\ max}$ = 2.39, 32.15°. Reflections collected = 82925, unique reflections = 25128 [*R*(int) = 0.0411]. Max./min. transmission = 0.801 and 0.744. Number of parameters = 1087, S = 1.038. Final *R* indices [*I*>2σ(*I*)] *R*1 = 0.0343, *wR*2 = 0.0677; *R* indices (all data) *R*1 = 0.0451, *wR*2 = 0.0718. Largest diff. peak and hole = 0.932 and -0.552 e. Å^{-3}.

[Er(Na·HOEt)(L)$_4$]$_2$. Empirical formula $C_{180}H_{132}Er_2Na_2O_{26}$; *MW* = 3091.35. λ = 1.54178 Å. Triclinic, Space group $P\bar{1}$, *a* = 13.9483(4), *b* = 14.5978(5), *c* = 18.0419(4) Å, α = 104.810(2)°, β = 90.329(2)°, γ = 89.553(2)°, Volume = 3551.42(18) Å^3, *Z* = 1; ρ_c = 1.445 Mg/m^3, μ = 2.812 mm^{-1}, crystal size 0.22 x 0.15 x 0.07 mm^3; $\theta_{min,\ max}$ = 2.53, 67.26°. Reflections collected = 35217, unique reflections = 12613 [*R*(int) = 0.0352]. Max./min. transmission = 0.829 and 0.670. Number of parameters = 951, S = 1.033. Final *R* indices [*I*>2σ(*I*)] *R*1 = 0.0363, *wR*2 = 0.0899; *R* indices (all data) *R*1 = 0.0408, *wR*2 = 0.0936. Largest diff. peak and hole = 1.639 and -0.573 e. Å^{-3}.

[Er(K·HOEt)(L)$_4$]$_2$·2(H$_2$O)(EtOH). Empirical formula $C_{182}H_{142}Er_2K_2O_{29}$; *MW* = 3205.68. λ = 0.71073 Å. Triclinic, Space group $P\bar{1}$, *a* = 14.9371(5), *b* = 15.5737(6), *c* = 18.1585(7) Å, α = 114.504(4)°, β = 91.285(3)°, γ = 98.795(3)°, Volume = 3781.1(2) Å^3, *Z* = 1; ρ_c = 1.408 Mg/m^3, μ = 1.233 mm^{-1}, crystal size 0.46 x 0.07 x 0.04 mm^3; $\theta_{min,\ max}$ = 2.28, 30.33°. Reflections collected = 36741, unique reflections = 20185 [*R*(int) = 0.0383]. Max./min. transmission = 0.954 and 0.745. Number of parameters = 990, S = 1.041. Final R indices [*I*>2σ(*I*)] *R*1 = 0.0427, *wR*2 = 0.0883; R indices (all data) *R*1 = 0.0544, *wR*2 = 0.0926. Largest diff. peak and hole = 1.076 and -0.653 e. Å^{-3}. The solvent molecules were modelled as an ethanol molecule disordered about a crystallographic inversion center and a water disordered over two sites with occupancies refined to 0.67(2) and its complement.

[Er(Rb·HOEt)(L)$_4$]$_2$. Empirical formula $C_{180}H_{132}Er_2O_{26}Rb_2$; *MW* = 3216.31. λ = 0.71073 Å. Triclinic, Space group $P\bar{1}$, *a* = 14.2006(3), *b* = 14.4538(4), *c* = 18.0067(4) Å, α = 102.245(2)°, β = 89.699(2)°, γ = 88.888(2)°, Volume = 3610.99(15) Å^3, *Z* = 1; ρ_c = 1.479

Mg/m^3, μ = 1.900 mm^{-1}, crystal size 0.31 x 0.19 x 0.06 mm^3; $\theta_{min,\ max}$ = 2.20, 29.00°. Reflections collected = 37245, unique reflections = 19183 [*R*(int) = 0.0298]. Max./min. transmission = 0.897 and 0.680. Number of parameters = 946, S = 1.092. Final *R* indices [*I*>2σ(*I*)] *R*1 = 0.0530, *wR*2 = 0.1226; *R* indices (all data) *R*1 = 0.0631, *wR*2 = 0.1270. Largest diff. peak and hole = 2.651 and -2.067 e. Å^{-3}.

[Yb(Na·HOEt)(L)$_4$]$_2$. Empirical formula $C_{180}H_{132}Na_2O_{26}Yb_2$; *MW* = 3102.91. λ = 0.71073 Å. Triclinic, Space group $P\bar{1}$. *a* = 14.0236(5), *b* = 14.5560(6), *c* = 18.0333(6) Å, α = 104.724(3)°, β = 90.128(3)°, γ = 89.234(3)°, Volume = 3559.9(2) Å^3, *Z* = 1; ρ_c = 1.447 Mg/m^3, μ = 1.389 mm^{-1}, crystal size 0.42 x 0.30 x 0.075 mm^3; $\theta_{min,\ max}$ = 2.749, 27.00°. Reflections collected = 58235, unique reflections = 15529 [*R*(int) = 0.0642]. Max./min. transmission = 0.901 and 0.643. Number of parameters = 951, S = 1.109. Final *R* indices [*I*>2σ(*I*)] *R*1 = 0.0531, *wR*2 = 0.1380; *R* indices (all data) *R*1 = 0.0582, *wR*2 = 0.1415. Largest diff. peak and hole = 4.980 and -2.350 e. Å^{-3}.

[Yb(K·HOEt)(L)$_4$]$_2$·2(H$_2$O)(EtOH). Empirical formula $C_{182}H_{142}K_2O_{29}Yb_2$; *MW* = 3217.24. λ = 1.54178 Å. Triclinic, Space group $P\bar{1}$, *a* = 14.9691(6), *b* = 15.5713(7), *c* = 18.1646(8) Å, α = 114.386(4)°, β = 91.488(4)°, γ = 98.946(4)°, Volume = 3790.1(3) Å^3, *Z* = 1; ρ_c = 1.410 Mg/m^3, μ = 3.326 mm^{-1}, crystal size 0.12 x 0.04 x 0.02 mm^3; $\theta_{min,\ max}$ = 3.00, 67.05°. Reflections collected = 40531, unique reflections = 13400 [*R*(int) = 0.0742]. Max./min. transmission = 1.00 and 0.89. Number of parameters = 991, S = 1.01. Final *R* indices [*I*>2σ(*I*)] *R*1 = 0.0442, *wR*2 = 0.0925; *R* indices (all data) *R*1 = 0.0624, *wR*2 = 0.0987. Largest diff. peak and hole = 0.898 and -0.757 e. Å^{-3}. The solvent molecules were modelled as an ethanol molecule disordered about a crystallographic inversion center and a water disordered over two sites with occupancies refined to 0.69(3) and its complement.

[Yb(Rb·HOEt)(L)$_4$]$_2$. Empirical formula $C_{180}H_{132}O_{26}Rb_2Yb_2$; MW = 3227.87. λ = 0.71073 Å. Triclinic, Space group $P\bar{1}$, *a* = 14.2183(4), *b* = 14.4303(3), *c* = 17.9542(5) Å, α = 102.094(2)°, β = 89.682(2)°, γ = 88.527(2)°, Volume = 3600.56(16) Å^3, Z = 1; ρ_c = 1.489 Mg/m^3, μ = 2.038 mm^{-1}, crystal size 0.33 x 0.15 x 0.09 mm^3; $\theta_{min,\ max}$ = 2.84, 31.97°. Reflections collected = 77555, unique reflections = 23506 [*R*(int) = 0.0470]. Max./min. transmission = 0.841 and 0.661. Number of parameters = 946, S = 1.064. Final *R* indices [I>2σ(I)] *R*1 = 0.0535, w*R*2 = 0.1246; *R* indices (all data) *R*1 = 0.0695, w*R*2 = 0.1331. Largest diff. peak and hole = 3.188 and -3.241 e. Å^{-3}.

Acknowledgments

M.M. wishes to thank the ARC for funding (FT1301000033) and E.G.M. gratefully acknowledges receipt of a Future Fellowship (FT100100795) from the ARC. B.L.R. wishes to thank Curtin University for the Australian Postgraduate Award and the University of Montreal (UdeM). G.S.H. thanks the Natural Sciences and Engineering Research Council of Canada and the Direction des Relations Internationales of UdeM. J.M.M. and M.C. thank Project Por Fesr-Tecnopolo AMBIMAT. The authors acknowledge access to the facilities at the Centre for Microscopy, Characterisation and Analysis, University of Western Australia. Simon W. Lewis and Reece D. Crocker of Curtin University are acknowledged for visible and NIR emission images.

Supporting Information

The Supporting information contains details of X-ray crystal structure molecular plots showing displacement ellipsoids at 50% probability level, Shape Version 2.1 data, solid state excitation spectra, solution state excitation and emission spectra, lifetime decays, and UV-visible absorption data.

References

[1] J.-C. G. Bünzli, C. Piguet, *Chem. Soc. Rev.* **2005**, *34*, 1048–1077.

[2] A. J. Amoroso, S. J. A. Pope, *Chem. Soc. Rev.* **2015**, DOI 10.1039/C4CS00293H.

[3] J. Lehr, P. D. Beer, S. Faulkner, J. J. Davis, *Chem. Commun.* **2014**, *50*, 5678–5687.

[4] K. Binnemans, *Chem. Rev.* **2009**, *109*, 4283–4374.

[5] J. Kido, Y. Okamoto, *Chem. Rev.* **2002**, *102*, 2357–2368.

[6] J. C. G. Bünzli, S. Comby, A. S. Chauvin, C. D. B. Vandevyver, *J. Rare Earth.* **2007**, *25*, 257–274.

[7] J. Andres, R. D. Hersch, J.-E. Moser, A.-S. Chauvin, *Adv. Funct. Mater.* **2014**, *24*, 5029–5036.

[8] S. V. Eliseeva, J.-C. G. Bünzli, *Chem. Soc. Rev.* **2010**, *39*, 189–227.

[9] J. C. G. Bünzli, S. V. Eliseeva, *J. Rare Earth.* **2010**, *28*, 824–842.

[10] J.-C. G. Bünzli, in *Lumin. Lanthan. Coord. Compd. Nanomater.* (Ed.: A. de Bettencourt-Dias), John Wiley & Sons Ltd, Chichester, United Kingdom, **2014**.

[11] J. V. Frangioni, *Curr. Opin. Chem. Biol.* **2003**, *7*, 626–634.

[12] A. de Bettencourt-Dias, *Dalton Trans.* **2007**, 2229–2241.

[13] S. Faulkner, S. J. A. Pope, B. P. Burton-Pye, *Appl. Spectrosc. Rev.* **2005**, *40*, 1–31.

[14] M. A. Katkova, M. N. Bochkarev, *Dalton Trans.* **2010**, *39*, 6599–6612.

[15] S. V. Eliseeva, J.-C. G. Bünzli, *New J. Chem.* **2011**, *35*, 1165–1176.

[16] J.-C. G. Bünzli, S. V Eliseeva, in *Compr. Inorg. Chem. II* (Eds.: J. Reedijk, K. Poeppelmeier), Elsevier, Amsterdam, Netherlands, **2013**, pp. 339–398.

[17] A. Beeby, I. M. Clarkson, R. S. Dickins, S. Faulkner, D. Parker, L. Royle, A. S. de Sousa, J. A. G. Williams, M. Woods, *J. Chem. Soc. Perkin Trans. 2* **1999**, *2*, 493–504.

[18] L. Winkless, R. H. C. Tan, Y. Zheng, M. Motevalli, P. B. Wyatt, W. P. Gillin, *Appl. Phys. Lett.* **2006**, *89*, 5–8.

[19] M. Giraud, E. S. Andreiadis, A. S. Fisyuk, R. Demadrille, J. Pécaut, D. Imbert, M. Mazzanti, *Inorg. Chem.* **2008**, *47*, 3952–3954.

[20] E. S. Andreiadis, D. Imbert, J. Pécaut, R. Demadrille, M. Mazzanti, *Dalton Trans.* **2012**, *41*, 1268–1277.

[21] E. R. Trivedi, S. V Eliseeva, J. Jankolovits, M. M. Olmstead, S. Petoud, V. L. Pecoraro, *J. Am. Chem. Soc.* **2014**, *136*, 1526–1534.

[22] A. Beeby, R. S. Dickins, S. Faulkner, D. Parker, J. A. Gareth Williams, *Chem. Commun.* **1997**, 1401–1402.

[23] J. Kim, Y. Park, *J. Korean Phys. Soc.* **2003**, *43*, 277–281.

[24] A. P. Bassett, R. Van Deun, P. Nockemann, P. B. Glover, B. M. Kariuki, K. Van Hecke, L. Van Meervelt, Z. Pikramenou, *Inorg. Chem.* **2005**, *44*, 6140–6142.

[25] P. B. Glover, A. P. Bassett, P. Nockemann, B. M. Kariuki, R. Van Deun, Z. Pikramenou, *Chem. Eur. J.* **2007**, *13*, 6308–6320.

[26] P. Martín-Ramos, M. Ramos Silva, F. Lahoz, I. R. Martín, P. Chamorro-Posada, M. E. S. Eusebio, V. Lavín, J. Martín-Gil, *J. Photochem. Photobiol. A Chem.* **2014**, *292*, 16–25.

[27] S. Biju, Y. K. Eom, J.-C. G. Bünzli, H. K. Kim, *J. Mater. Chem. C* **2013**, *1*, 6935.

[28] R. H. C. Tan, M. Motevalli, I. Abrahams, P. B. Wyatt, W. P. Gillin, *J. Phys. Chem. B* **2006**, *110*, 24476–24479.

[29] P. Martín-Ramos, P. S. Pereira da Silva, V. Lavín, I. R. Martín, F. Lahoz, P. Chamorro-Posada, M. R. Silva, J. Martín-Gil, *Dalton Trans.* **2013**, *42*, 13516–26.

[30] T.-S. Kang, B. S. Harrison, M. Bouguettaya, T. J. Foley, J. M. Boncella, K. S. Schanze, J. R. Reynolds, *Adv. Funct. Mater.* **2003**, *13*, 205–210.

[31] M. A. Katkova, A. P. Pushkarev, T. V. Balashova, A. N. Konev, G. K. Fukin, S. Y. Ketkov, M. N. Bochkarev, *J. Mater. Chem.* **2011**, *21*, 16611–16620.

[32] S. Comby, J.-C. G. Bünzli, in *Handb. Phys. Chem. Rare Earths* (Eds.: K.A. Gschneidner, J.-C.G. Bünzli, V.K. Pecharsky), Elsevier B.V., Amsterdam, The Netherlands, **2007**, pp. 217–470.

[33] B. L. Reid, S. Stagni, J. Malicka, M. Cocchi, G. S. Hanan, M. I. Ogden, M. Massi, *Chem. Commun.* **2014**, *50*, 11580–11582.

[34] K. Binnemans, in *Handb. Phys. Chem. Rare Earths* (Eds.: K.A. Gschneidner, J.-C.G. Bunzli, V.J. Pecharsky), Elsevier B.V., Amsterdam, The Netherlands, **2005**, pp. 107–272.

[35] M. Ismail, S. J. Lyle, J. E. Newbery, *J. Inorg. Nucl. Chem.* **1969**, *31*, 2091–2093.

[36] G. A. Crosby, R. E. Whan, *J. Chem. Phys.* **1960**, *32*, 614–615.

[37] G. A. Crosby, R. E. Whan, R. M. Alire, *J. Chem. Phys.* **1961**, *34*, 743–748.

[38] M. Llunell, D. Casanova, J. Cirera, P. Alemany, S. Alvarez, "Shape version 2.1," can be found under http://www.ee.ub.es/index.php/news-ee/575-shape-available, **2013**.

[39] D. Casanova, M. Llunell, P. Alemany, S. Alvarez, *Chem. Eur. J.* **2005**, *11*, 1479–1494.

[40] N. M. Shavaleev, R. Scopelliti, F. Gumy, J.-C. G. Bünzli, *Inorg. Chem.* **2009**, *48*, 7937–7946.

[41] M. Mehlstäubl, G. S. Kottas, S. Colella, L. De Cola, *Dalton Trans.* **2008**, *2*, 2385–2388.

[42] X. Yang, D. Schipper, R. A. Jones, L. A. Lytwak, B. J. Holliday, S. Huang, *J. Am. Chem. Soc.* **2013**, *135*, 8468–8471.

[43] A. P. Pushkarev, V. A. Ilichev, T. V. Balashova, D. L. Vorozhtsov, M. E. Burin, D. M. Kuzyaev, G. K. Fukin, B. A. Andreev, D. I. Kryzhkov, A. N. Yablonskiy, et al., *Russ. Chem. Bull.* **2013**, *62*, 392–397.

[44] W. D. Horrocks, J. P. Bolender, W. D. Smith, R. M. Supkowski, *J. Am. Chem. Soc.* **1997**, *119*, 5972–5973.

[45] M. Asano-Someda, Y. Kaizu, *J. Photochem. Photobiol. A Chem.* **2001**, *139*, 161–165.

[46] M. H. V. Werts, R. T. F. Jukes, J. W. Verhoeven, *Phys. Chem. Chem. Phys.* **2002**, *4*, 1542–1548.

[47] N. M. Shavaleev, R. Scopelliti, F. Gumy, J.-C. G. Bünzli, *Inorg. Chem.* **2009**, *48*, 2908–2918.

[48] H. Q. Ye, Z. Li, Y. Peng, C. C. Wang, T. Y. Li, Y. X. Zheng, A. Sapelkin, G. Adamopoulos, I. Hernández, P. B. Wyatt, et al., *Nat. Mater.* **2014**, *13*, 382–386.

[49] S. Sato, M. Wada, *Bull. Chem. Soc. Jpn.* **1970**, *43*, 1955–1962.

[50] A. De Bettencourt-Dias, P. S. Barber, S. Bauer, *J. Am. Chem. Soc.* **2012**, *134*, 6987–6994.

[51] A. de Bettencourt-Dias, in *Lumin. Lanthan. Ions Coord. Compd. Nanomater.* (Ed.: A. de Bettencourt-Dias), Elsevier B.V., Amsterdam, The Netherlands, **2014**, pp. 1–48.

[52] S. Cotton, *Lanthanide and Actinide Chemistry*, John Wiley & Sons, Ltd, Chichester, UK, **2006**.

[53] S. Petit, F. Baril-Robert, G. Pilet, C. Reber, D. Luneau, *Dalton Trans.* **2009**, 6809–6815.

[54] N. M. Shavaleev, S. V Eliseeva, R. Scopelliti, J.-C. G. Bünzli, *Inorg. Chem.* **2014**, *53*, 5171–5178.

[55] N. M. Shavaleev, S. V. Eliseeva, R. Scopelliti, J. C. G. Bünzli, *Chem. Eur. J.* **2009**, *15*, 10790–10802.

[56] W. D. Horrocks, D. R. Sudnick, *Acc. Chem. Res.* **1981**, *14*, 384–392.

[57] P. C. Andrews, W. J. Gee, P. C. Junk, M. Massi, *New J. Chem.* **2013**, *37*, 35–48.

[58] S. I. Klink, G. A. Hebbink, L. Grave, P. G. B. Oude Alink, F. C. J. M. Van Veggel, M. H. V. Werts, *J. Phys. Chem. A* **2002**, *106*, 3681–3689.

[59] G. M. Sheldrick, *Acta Crystallogr. Sect. C Struct. Chem.* **2015**, *71*, 3–8.

Graphical Abstract

Lanthanoid/Alkali Metal β-Triketonate Assemblies: A Robust Platform for Efficient NIR Emitters

Mr. Brodie L. Reid,[a] Dr. Stefano Stagni,[b] Dr. Joanna M. Malicka,[c] Dr. Massimo Cocchi,[c,d] Dr. Alexandre N. Sobolev,[e] Prof. Brian W. Skelton,[e] Dr. Evan G. Moore,[f] Prof. Garry S. Hanan,[g] Prof. Mark I. Ogden,*[a] and Dr. Massimiliano Massi*[a]

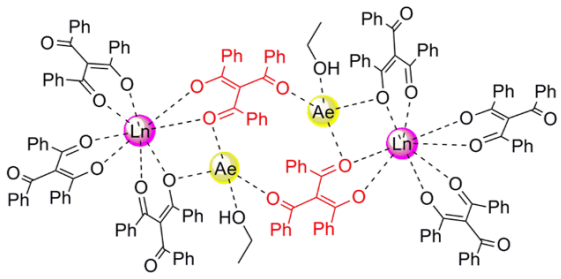

$[Ln(Ae{\cdot}HOEt)(\mathbf{L})_4]_2$

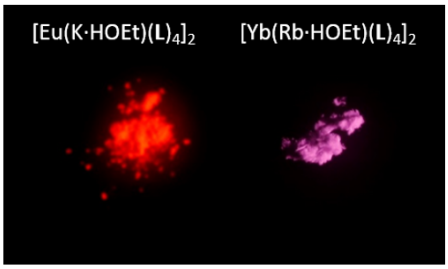

The reaction of hydrated $LnCl_3$, an alkali metal hydroxide, and tribenzoylmethane affords a series of lanthanoid/alkali metal tetranuclear assemblies (Ln = Eu, Er, Yb; Ae = Na, K, Rb). In the solid state the complexes are emissive, with the NIR emitting Yb^{3+} and Er^{3+} species presenting excited-state lifetimes which outclass all other species in the β-diketonate class in even when the ligands have been perfluorinated to reduce the effect of multiphonon relaxation. This result opens the door for the β-triketonate class of ligand to be a viable alternative to β-diketonates in the field of light emitting technologies.